Third International Symposium on Marine Propulsors
smp'13, Launceston, Tasmania, Australia, May 2013

URANS Simulations of Cavitation and Hull Pressure Fluctuation for Marine Propeller with Hull Interaction

Kwang-Jun Paik, Hyung-Gil Park, Jongsoo Seo

Samsung Ship Model Basin (SSMB), Samsung Heavy Industries Co., Ltd., Daejeon, Korea

ABSTRACT

Simulations of cavitation flow and hull pressure fluctuation for a marine propeller operating behind a hull using the unsteady Reynolds-Averaged Navier-Stockes (URANS) are presented. A full hull body submerged under the free surface is modeled in the computational domain to simulate directly the wake field of the ship at the propeller plane. A symmetry boundary condition is applied on the top of computational domain instead of the free surface, which is similar to a cavitation tunnel. To observe the cavitation pattern during the revolution of propeller, the propeller is rotated with a constant rotation angle of 1.5° using a sliding mesh technique. Simulations are performed in design and ballast draught conditions to study the effect of cavitation number. And two propellers with slightly different geometry are simulated to validate the detectability of the numerical simulation. All simulations are performed using a commercial CFD software FLUENT. Cavitation patterns of the simulations are compared with the experimental results carried out in Samsung CAvitation Tunnel (SCAT). Simulation results for the hull pressure fluctuation induced by a propeller are also compared with the experimental results with good agreement.

Keywords

Propeller, Cavitation, Hull pressure fluctuation, URANS, Propeller-hull interaction

1 INTRODUCTION

The practical importance of accurate numerical simulation to predict the cavitation pattern and hull pressure amplitude has been increased in the field of ship building industries. The researches to simulate the cavitation flow using RANS solver were performed actively in the last several years because cavitation models for RANS solver and computation power have been rapidly developed in the last decade.

Watanabe et al. (2003) started the study on the cavitation flow for a marine propeller using RANS. Salvatore et al. (2009) compared seven computational models using RANS, LES, and BEM for the INSEAN E779A propeller in uniform flow and wake field. The cavitation simulation for conventional and highly-skewed propellers in the behind-hull condition using an in-house RANS solver was performed by Shin et al. (2011). Hasuike et al. (2010) simulated the cavitation flow and showed a possibility to predict the cavitation erosion risk with the indexes using time differential of cavity void fraction or pressure.

On the other hand, the usage of commercial CFD software was gradually increased to simulate the cavitation flow for marine propellers. Boorsma & Whitworth (2011) used STAR-CCM+ to study on the prediction of cavitation and erosion for a propeller and rudder. Bertetta et al. (2011) compared the results of RANS solver using STAR-CCM+ with those of potential solver for the cavitation flow of a controllable pitch propeller. Morgut & Nobile (2011) studied on the performance of three cavitation models for a marine propeller using ANSYS-CFX. Li & Terwisga (2011) used FLUENT to investigate unsteady cavitation phenomena for 2D and 3D foils. Kawamura (2010) assessed cavitation erosion risk based on pressure impacts and simulated the cavitation flow and the magnitude of pressure amplitude for a marine propeller using FLUENT.

Most of simulations except for Kawamura (2010) prescribed a velocity distribution at the inlet boundary of the computational domain to achieve the correct wake field at the propeller plane. In that case, the adjustment of inlet boundary condition to get a desired velocity contour at propeller plane is of primary importance and very laborious work. Therefore, Kawamura (2010) used a full hull body to generate the wake field. Nevertheless, the cavity extent was under-predicted and the pressure amplitudes were about 70% of the experimental results.

In this paper the results of numerical simulations using URANS for the cavitation pattern and hull pressure fluctuation of marine propellers are presented. A commercial CFD software FLUENT version 14.0 is used for the numerical simulations. Schneer & Sauer (2001) cavitation model is applied to simulate the cavitation flow. A computational domain including a full hull body submerged under the free surface is used to simulate directly the wake field at the propeller plane. Two kinds of studies varying cavitation number and propeller geometry are executed in order to validate the numerical simulation method. And the numerical simulations are

performed at the same as the test conditions in the cavitation tunnel and compared with the experimental results.

2 NUMERICAL METHODS AND MODELS

A commercial CFD software FLUENT version 14.0 was used for the numerical simulations, in which the cavitation flow was solved by a mixture model based on a single-fluid multiphase mixture flow approach.

2.1 Governing Equations

In the mixture model, the continuity equation and the momentum equation become as

$$\frac{\partial}{\partial t}(\rho_m)+\nabla\cdot(\rho_m\vec{v}_m)=0 \tag{1}$$

$$\frac{\partial}{\partial t}(\rho_m\vec{v}_m)+\nabla\cdot(\rho_m\vec{v}_m\vec{v}_m) = -\nabla p+\nabla\cdot\left[\mu_m\left(\nabla\vec{v}_m+\nabla\vec{v}_m^{T}\right)\right]+\rho_m\vec{g}+\vec{F} \tag{2}$$

The mixture density and viscosity coefficient are defined as

$$\begin{aligned}\rho_m &= \alpha\rho_v+(1-\alpha)\rho_l \\ \mu_m &= \alpha\mu_v+(1-\alpha)\mu_l\end{aligned} \tag{3}$$

where α is the vapor volume fraction. Subscripts m, v, and l represent mixture, vapor, and liquid phase, respectively.

2.2 Cavitation Model

Schneer & Sauer (2001) cavitation model applied in this research solves the vapor volume fraction with following transport equation:

$$\frac{\partial}{\partial t}(\alpha\rho_v)+\nabla\cdot(\alpha\rho_v\vec{v}_v)=R_e-R_c \tag{4}$$

where the terms, R_e and R_c, account for the mass transfer between the liquid and vapor phase in cavitation denoting the evaporation and condensation of the vapor bubbles. The forms of R_e and R_c are written as follows:

when $p_v \geq p$,

$$R_e=\frac{\rho_v\rho_l}{\rho_m}\alpha(1-\alpha)\frac{3}{R_B}\sqrt{\frac{2}{3}\frac{(p_v-p)}{\rho_l}} \tag{5}$$

when $p_v \leq p$,

$$R_c=\frac{\rho_v\rho_l}{\rho_m}\alpha(1-\alpha)\frac{3}{R_B}\sqrt{\frac{2}{3}\frac{(p-p_v)}{\rho_l}}. \tag{6}$$

Here, the bubble radius, R_B, is expressed as

$$R_B=\left(\frac{\alpha}{1-\alpha}\frac{3}{4\pi}\frac{1}{n_b}\right)^{\frac{1}{3}} \tag{7}$$

where n_b is the bubble number density.

3 MODEL TEST

Model tests to observe cavitation flow on a propeller blade and to measure pressure fluctuation on a hull surface induced by the propeller cavitation were carried out in Samsung CAvitation Tunnel (SCAT). The principal particulars of the test section of SCAT are summarized in Table 1 and the set-up of a model ship and propeller is shown in Figure 1. The definition of propeller blade angle is depicted in Figure 2. The propeller blade angle begins from the top position toward propeller rotation direction. Pressure transducers to measure the pressure fluctuation on a hull surface were installed on the top of propeller with the intervals of 30mm as illustrated in Figure 3.

Table 1: Principal particulars of the test section of SCAT

Item	Value
Dimension of Test Section (L × B × D)	12.0 × 3.0 × 1.4 m
Maximum Speed	12.0 m/s
Contraction Ratio	2.75

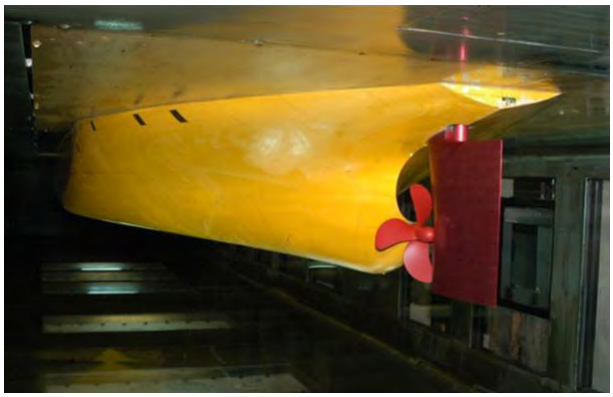

Figure 1: Set-up of model ship and propeller in SCAT

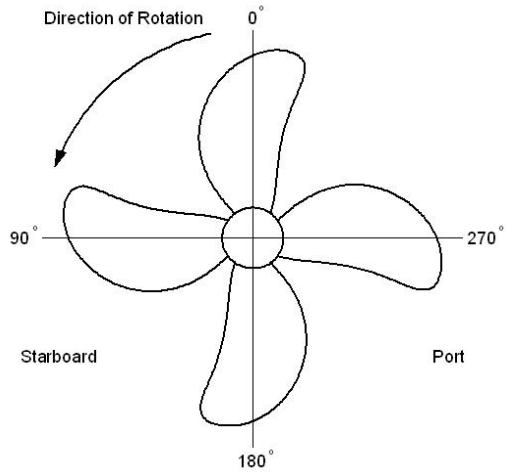

Figure 2: Definition of propeller blade angle

The length of the model ship, a crude oil tanker, was about 7.6m/s and the diameter of the model propeller was 226.1mm in this research. The blockage of the test section due to the model ship was about 13.2%. The surface of the model propeller was coated with a rough paint to stabilize the behavior of cavitation flow. The inflow velocity of model test was fixed as 5.5m/s. The propeller rotation speed was set with the thrust identity method based on the results of self-propulsion test in a towing tank.

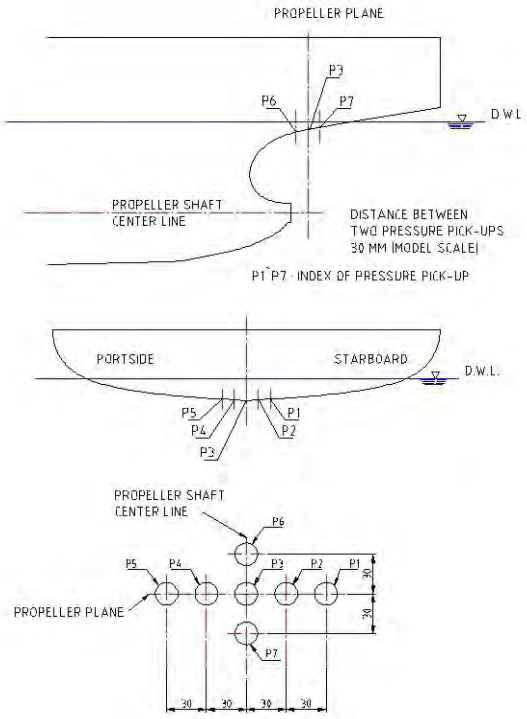

Figure 3: Position of pressure transducers installed on a model ship

4 NUMERICAL SIMULATION

4.1 Grid System

To simulate the propeller cavitation flow under similar situation to the model test, a full hull body submerged under the free surface was modeled in the computational domain. The free surface was substituted with a symmetry boundary condition because the mixture model for the cavitation flow and the Volume of Fluid (VOF) model for the free surface could not be implemented simultaneously in FLUENT.

A sliding block surrounding the propeller, composed of unstructured girds, was applied to implement the effect of propeller rotation. Pyramid cells were used for the surface of propeller and boundaries, and tetrahedral cells were filled in the block. On the other hand, structure girds were applied to the other domains expect for the sliding block. Figure 4 shows the outline of grid system including boundary conditions. The grid sizes were 1.4M and 2.6M cells for the sliding block and the other blocks, respectively.

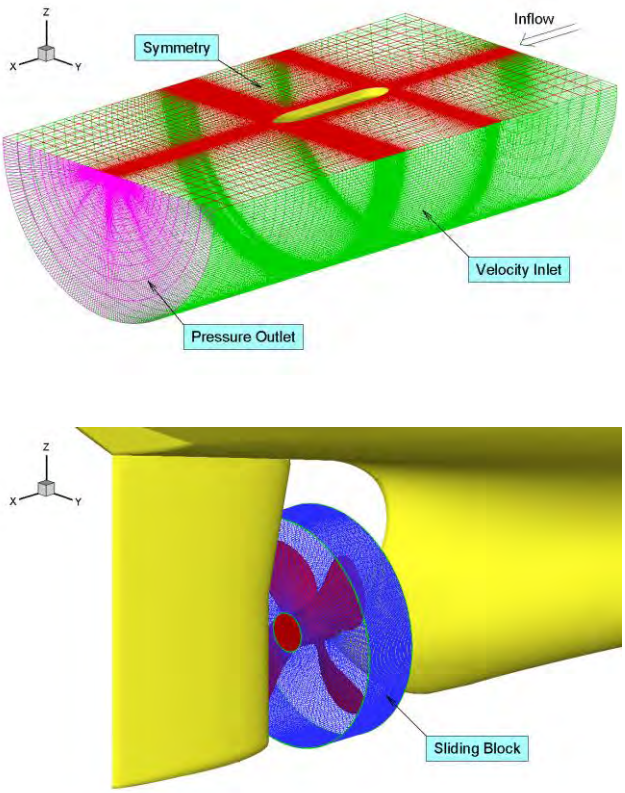

Figure 4: Outline of grid system and boundary conditions for computational domain and propeller block

4.2 Simulation Method

As the numerical model for cavitation flow, Schneer & Sauer (2001) was applied in this research. Bubble number density was set as 1e+15. To improve the convergency of cavitation flow and reduce the computational time, Multiple Reference Frame (MFR) was used at first and Sliding Mesh Model (SMM) was then applied to simulate the rotation of propeller. Propeller rotated with a constant time step corresponding to the rotating angle of 1.5°. Time histories of fluctuating pressure on the hull surface were recorded to compare with the experimental results at the same positions as the pressure transducers installed on the model test. The simulation methods applied in this research are summarized in Table 2.

Table 2: Summary of simulation methods

Item	Method
Governing Equation	RANS
Turbulence Model	RSM
Cavitation Model	Mixture
P-V Coupling	SIMPLEC
Pressure Solver	Standard
Momentum Solver	Second Order Upwind

A propeller coated with the rough paint tended to increase the cavity extent and pressure pulse as compared with a smooth surface propeller in the experiment. However, since it was impossible that the effect of the paint was implemented in numerical simulation, a smaller cavitation number was used for the simulation instead of the rough paint. The adjustment was approached with ignoring a wave height at stern which was considered in the model test.

5 RESULTS AND DISCUSSION

In this research two kinds of simulations were executed and compared with the experimental results. The first simulation was performed at two draught conditions to investigate the effect of cavitation number. The other study was to validate the detectability of the numerical simulation about the differences of cavitation pattern and pressure amplitude from the small modification of propeller geometry.

Prior to the cavitation simulation, the bare hull without the propeller was simulated to compare the wake field at the propeller plane. Figure 5 shows the comparison of velocity contours and vectors between the experimental data and simulation result at the propeller plane. Inlet velocity of the numerical simulation was 5.5m/s, which was the same velocity as the experiment. The velocity contour and vector are normalized by the inlet velocity. The pattern of the wake fields is similar to each other. However, the axial velocity of the experiment at outer radii of lower part is about 0.1 higher than the simulation because the velocity at lower part is probably accelerated due to the blockage effect at the experiment. The hook shape vortex generated by bilge vortex is appeared around 20° in the experiment, while it is not observed in the simulation.

5.1 Draught Condition

The simulations were performed at design and ballast draught conditions, and the simulation results were compared with the experimental results of SCAT. The model propeller, tested in the model test, is a 4-blade propeller (Prop-A) designed for a crude oil tanker. Mean pitch ratio and expanded area ratio of the propeller are 0.655 and 0.480, respectively. The simulation conditions are summarized in Table 3. The cavitation number is defined as

$$\sigma = \frac{p - p_v}{0.5\rho n^2 D^2} \qquad (8)$$

where p is a static pressure at the 70% of propeller radius above the propeller center and p_v is a vapor pressure. n and D are a propeller rotation speed and a propeller diameter, respectively.

The thrusts of the simulations at the design and ballast conditions were about 4% higher than those of the experiments. The larger thrusts of the simulations result from the slower axial velocity at the propeller plane as compared in Figure 5.

Cavitation patterns at the propeller blade angle of 0°, 20°, and 40° at the design and ballast draught conditions are compared with the experimental results in Figures 6 and 7. The cavity extent in the simulation are expressed with the isosurface of α =0.1. The simulation results have some limitations to capture the tip vortex cavitation, but the cavity patterns generally well agree with the experiments. At the design draught condition, the leading edge cavitation near 0.8R of the propeller blade is not appeared in the numerical simulation, while it is observed with very unstable behavior in the experiment. At the ballast draught condition, the cavity extents at all blade angles well correspond with the experiments. The sheet cavitation was not appeared in the range between 90° and 330° in the experiments, but it was observed until about 240° in the simulations due to the slower axial velocity than the experiment as shown in Figure 5.

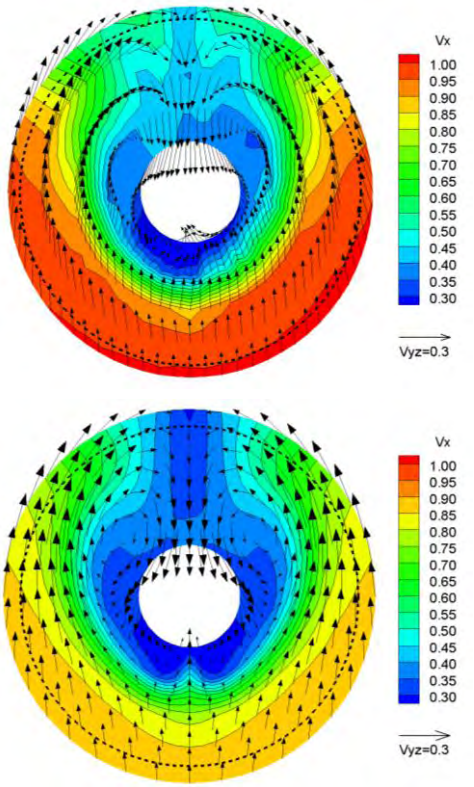

Figure 5: Velocity contours and vectors of experiment (top) and simulation (bottom) at propeller plane (dashed circle: outline of propeller disk)

Table 3: Summary of simulation conditions to study the effect of draught condition

	Design	Ballast
Inflow Speed	5.5 m/s	
Propeller Diameter	226.1 mm	
Propeller Speed	38.0 rps	39.3 rps
Cavitation Number	2.129	1.462

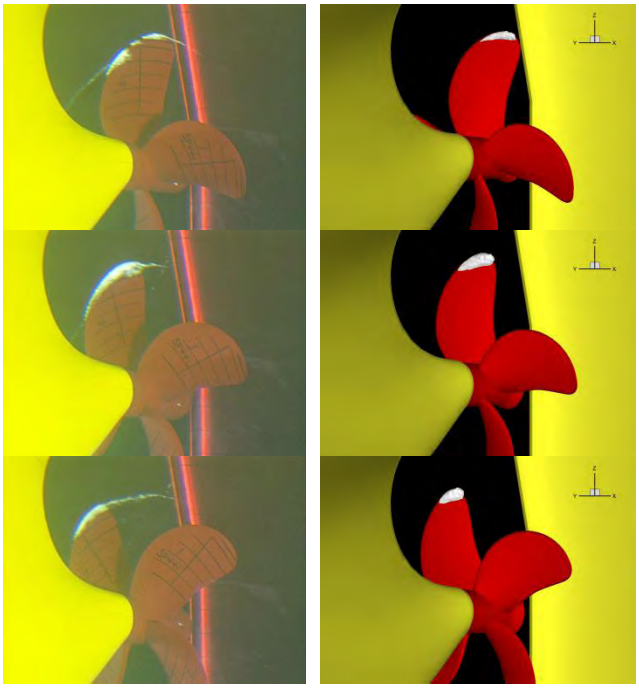

Experiment Simulation

Figure 6: Comparison of cavitation patterns at design drauhgt condition for Prop-A (top:0°, middle:20°, bottom: 40°)

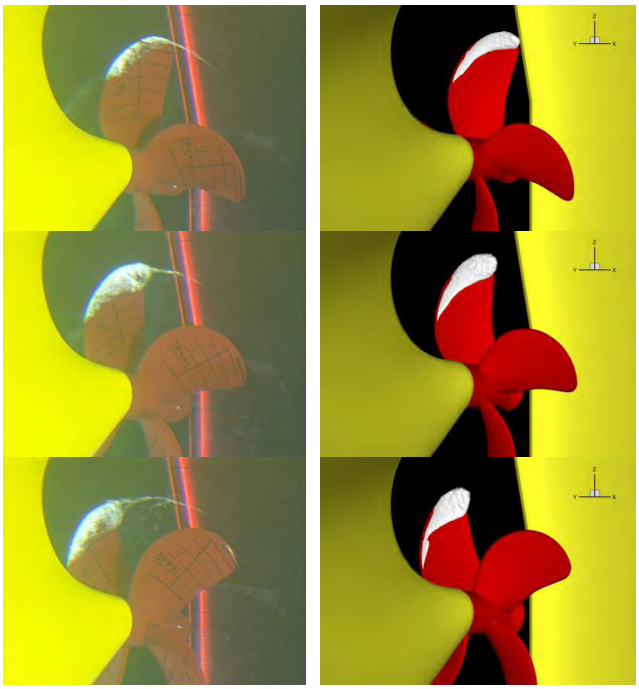

Experiment Simulation

Figure 7: Comparison of cavitation patterns at ballast drauhgt condition for Prop-A (top:0°, middle:20°, bottom: 40°)

Figure 8 shows an instantaneous pressure distribution on the hull surface induced by the propeller cavitation. Very high pressure concentrates above the propeller position, especially on starboard side rather than port side. Time histories of pressure pulse on P2 transducer at the design and ballast draught conditions are plotted in Figure 9. Hull pressure pulse is expressed with the pressure pulse coefficient defined as

$$K_P = \frac{\Delta p}{\rho n^2 D^2} \tag{9}$$

where Δp is the pressure fluctuation amplitude from the mean pressure. The pressure fluctuation at the design draught condition has eight peaks during one revolution, while that at the ballast draught condition has four peaks.

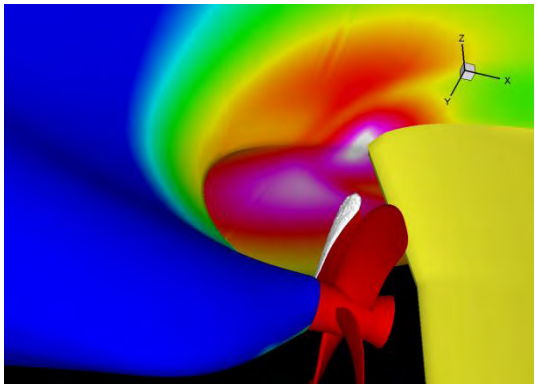

Figure 8: Instantaneous pressure distribution on the hull surface induced by the propeller cavitation

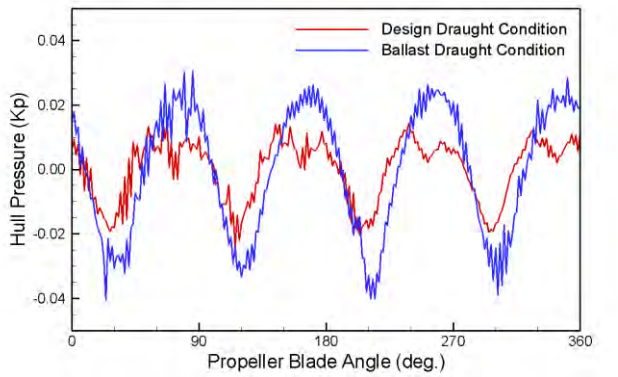

Figure 9: Time history comparison of pressure fluctuation of P2 transducer at ballast and ballast draught conditions for Prop-A

The hull pressure amplitudes for Prop-A at the design draught condition are compared with the experimental results in Figure 10. Since the position of P7 was concealed beneath the rudder trunk, P7 could not be measured in this research. For the first blade frequency (1BF), the simulation results show good agreement with the experimental results in the tendency and magnitude of pressure fluctuation, but the pressure amplitudes of P1 and P2 at starboard side are about 20% and 10% higher than the experiments, respectively. At the other pressure transducers, the pressure amplitudes are very similar to the experiments. The second blade frequencies (2BF) of the simulation are almost half of the experimental results,

even though the tendency is similar to the experiments. As explained in Figure 5, the gradient of axial velocity due to the hook shape vortex probably affects the increase of 2BF amplitude in the experiment. In contrast, the velocity gradient is very smooth in the simulation, resulting in relatively small amplitude of 2BF. Overall, the hull pressure amplitudes of starboard side are higher than port side, and the pressure amplitude of P6 located upstream from the propeller plane is higher than P3 located at the propeller plane.

Figure 11 shows the comparison of the hull pressure amplitudes at the ballast draught condition with the experimental results. The amplitudes of 1BF are about 10% higher than the experiments except for P1 and P6. The pressure amplitude of P1 is about 28% higher than the experiment, while that of P6 is about 5% lower. Nevertheless, the tendency of pressure amplitude is very close to the experiment. However, the amplitudes of 2BF are significantly lower than the experiments because the effect of axial velocity gradient in the simulation may be diminished due to the relatively large cavity extent in the ballast draught condition. This phenomenon can be explained through Figure 9. The two peaks with about 40° interval at the crest of the signal observed in the design load condition is not observed in the ballast condition.

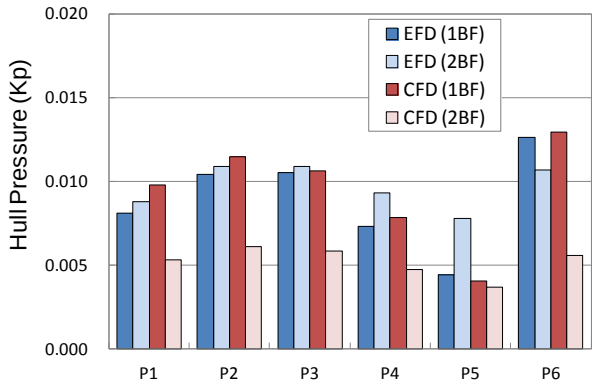

Figure 10: Comparison of pressure amplitudes at design druaght condition for Prop-A

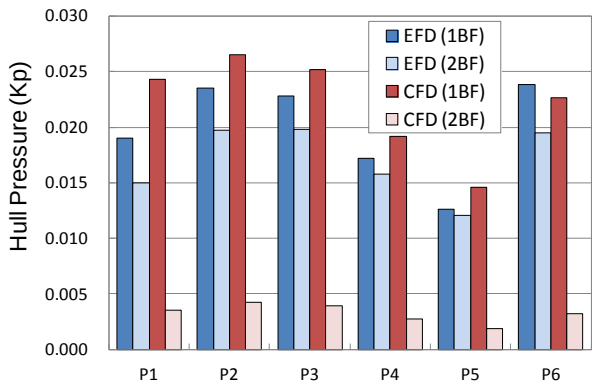

Figure 11: Comparison of pressure amplitudes at ballast druaght condition for Prop-A

5.2 Propeller Geometry

Another propeller (Prop-B) was designed to study on the effect of propeller rake distribution. Prop-B has the backward rake of 0.014D at tip, while Prop-A has the forward rake of 0.007D at tip. The other parameters for propeller geometry such as pitch, camber, and chord including propeller diameter are exactly same. Due to the rake distribution, the rotation speed of Prop-B is slightly higher than that of Prop-A; as a result, the cavitation number of Prop-B is relatively lower than that of Prop-A. The simulation conditions for Prop-A and Prop-B are summarized in Table 4.

Table 4: Summary of simulation conditions to study the effect of propeller geometry

	Prop-A	Prop-B
Inflow Speed	5.5 m/s	
Propeller Diameter	226.1 mm	
Propeller Speed	39.3 rps	40.6 rps
Cavitation Number	1.462	1.455

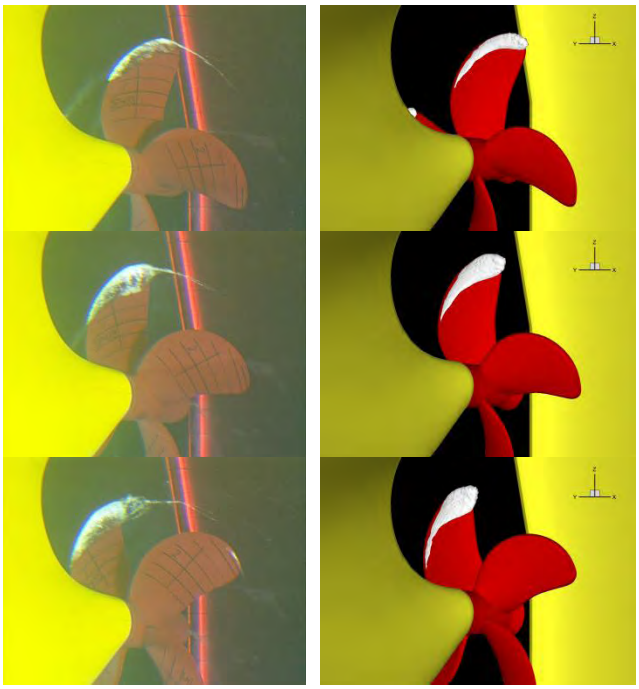

Experiment Simulation

Figure 12: Comparison of cavitation patterns at ballast drauhgt condition for Prop-B (top:0°, middle:20°, bottom: 40°)

The cavitation patterns at the ballast draught condition for Prop-B are compared with the experimental results in Figure 12. The cavity extents of Prop-B are not different from Prop-A in both experiment and simulation. However, the effect of propeller rake is distinguished in the hull pressure amplitude as shown in Figure 13. Prop-B

with the backward rake reduces the pressure amplitude of about 5% at P1 to P3 and about 13% at P4 and P5 in the experiment. Similarly, the amounts of reduction are about 10% at P1 to P3, about 5% at P4 and about 10% at P5 in the simulation. From the simulation results, it can be concluded that the numerical simulation using URANS is useful to detect the difference of pressure amplitude due to the small modification of propeller geometry.

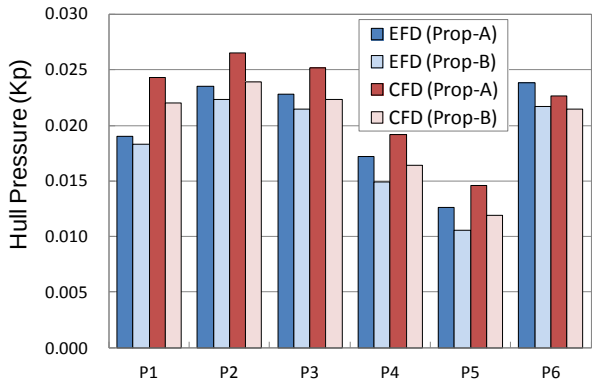

Figure 13: Comparison of 1BF pressure amplitudes between Prop-A and Prop-B at ballast condition

6 CONCLUSIONS

Numerical simulation studies using URANS for cavitation flow and hull pressure fluctuation of marine propellers were presented in this paper. A computational domain including a full hull body submerged under the free surface was used to simulate directly the wake field at the propeller plane. And the simulation results were compared with the experimental results performed in the cavitation tunnel.

Two kinds of studies were executed in this research. At first, the numerical simulations were performed in design and ballast draught conditions to study the effect of cavitation number. The cavitation patterns at both conditions agreed well with the experimental results. The first blade frequencies of the pressure fluctuations in the simulations were slightly larger than the experiments, whereas the tendency of the pressure amplitudes according to the location of the transducers was very similar to the experiments. However, for the second blade frequencies the simulations showed some limitations to predict the magnitude of pressure fluctuation due to the difference of wake field at the propeller plane. The other study was to validate the detectability of the numerical simulation for the cavitation pattern and hull pressure amplitude. Two propellers with slightly different geometry were simulated and compared with the experimental results. The cavity extents of the simulation and experiment were not different between two propellers. However, the pressure amplitudes of two propellers had small difference, and that was validated in the numerical simulation.

In conclusion, the cavitation simulation using URANS showed reliable performance to predict the cavitation pattern and hull pressure amplitude through this research. To improve the accuracy of 2BF harmonics in the simulation, however, numerical methods to achieve more accurate wake field at the propeller plane need to be studied in detail.

For the further work, various ship types will be simulated and compared with experimental data to evaluate this numerical simulation method.

ACKNOWLEDGEMENTS

This work was partially carried out in the research grant (No. 2011-10040081) funded by the Korean Ministry of Knowledge Economy.

REFERENCES

Bertetta, D., Brizzolara, S., Gaggero, S., Savio, L. & Viviani, M. (2011). 'Numerical and Experimental Characterization of a CP Propeller Unsteady Cavitation at Different Pitch Settings'. Second International Symposium on Marine Propulsors, Hamburg, Germany.

Boorsma, A. & Whitworth, S. (2011). 'Understanding Details of Cavitation'. Second International Symposium on Marine Propulsors, Hamburg, Germany.

Hasuike, N., Yamasaki, S., Ando, J. & Okazaki, A. (2010). 'Numerical Study on Cavitation Erosion Risk of Marine Propellers Operating in Wake Flow', International Propulsion Symposium, Okayama, Japan.

Kawamura, T. (2010). 'Numerical Simulation of Propulsion and Cavitation Performance of Marine Propeller'. International Propulsion Symposium, Okayama, Japan.

Li, Z. & Terwisga, T. (2011). 'On the Capability of Multiphase RANS Codes to Predict Cavitation Erosion'. Second International Symposium on Marine Propulsors, Hamburg, Germany.

Morgut, M. & Nobile, E. (2011). 'Influence of the Mass Transfer Model on the Numerical Prediction of the Cavitating Flow Around a Marine Propeller'. Second International Symposium on Marine Propulsors, Hamburg, Germany.

Salvatore, F., Streckwall, H. & van Terwisga, T. (2009). 'Propeller Cavitation Modelling by CFD - Results from the VIRTUE 2008 Rome Workshop'. First International Symposium on Marine Propulsors, Trondheim, Norway.

Shin, K. W., Anderson, P. & Mikkelsen, R. (2011). 'Cavitation Simulation on Conventional and High-Skewed Propellers in the Behind-Hull Condition'. Second International Symposium on Marine Propulsors, Hamburg, Germany.

Schneer, G. H. & Sauer, J. (2001). 'Physical and Numerical Modeling of Unsteady Cavitation Dynamics'. 4th International Conference on Multiphase Flow, Orleans, United States.

Watanabe, T., Kawamura, T., Takekoshi, Y., Maeda, M. & Rhee, S. H. (2003). 'Simulation of Steady and Unsteady Cavitation on a Marine Propeller Using a RANS CFD Code'. Fifth International Symposium on Cavitation (CAV2003), Osaka, Japan.